JOURNAL OF SOLID STATE CHEMISTRY 116, 385–391 (1995)

Influence of Oxygen and Strontium Content on the $Pr_{2-y}Sr_yCuO_{4-\delta}$ System

A. Varela,* M. Vallet-Regí,†,‡ and J. M. González-Calbet*,‡,[1]

*Departamento de Química Inorgánica, Facultad de Químicas, Universidad Complutense, 28040 Madrid, Spain;
†Departamento de Química Inorgánica y Bioinorgánica, Facultad de Farmacia, Universidad Complutense, 28040 Madrid, Spain; and
‡Instituto de Magnetismo Aplicado "Salvador Velayos," Apdo. Correos 155, Las Rozas, 28230 Madrid, Spain

Received August 3, 1994; in revised form November 14, 1994; accepted November 16, 1994

Samples of the $Pr_{2-y}Sr_yCuO_{4-\delta}$ system have been prepared with accurate control of the oxygen content. T′–T*–T–Sr_2CuO_3 single phases are only obtained in air for $y = 0$, 0.4, 1, and 2, respectively. The microstructural study indicates that oxygen vacancies are randomly disordered for $y = 0.4$ ($Pr_{1.6}Sr_{0.4}CuO_{3.94}$) but an incommensurable modulated structure appears for $y = 1$ ($PrSrCuO_{3.6}$) as a consequence of ordering of anionic vacancies along [110]. Two new materials are obtained when air-synthesized materials are annealed under oxygen atmosphere. For $y = 0.45$, an orthorhombic T* phase is isolated. For $y = 1$, a material showing ordered oxygen vacancies in the basal Cu–O planes is described. © 1995 Academic Press, Inc.

1. INTRODUCTION

Three different related structures (**T**, **T′**, **T***) have been reported in system R_2CuO_4 (R = rare-earth), which depend on the specific atomic radius of R cations occupying A positions of the ABO_3 perovskite-type substructure (Fig. 1). These structures differ significantly in the oxygen coordination around copper: octahedral in **T** phase and planar in **T′** phase. The **T*** structure, however, is composed of **T**- and **T′**-type slabs alternating along the [001] direction, which leads to a pyramidal oxygen coordination around the copper atoms.

Hole doping in La_2CuO_4 leads to a superconducting $La_{2-y}Sr_yCuO_4$ material for $y = 0.2$, the **T**-type structure (with orthorhombic distortion or superstructures) being maintained in a wide compositional range $0 \leq y \leq 1.34$ (1, 2). For $y > 1.34$, a mixture of the **T**-type phase and Sr_2CuO_3 (213) is obtained.

A structural study of the Nd_2CuO_4–Sr_2CuO_3 system (3) suggests that $Nd_{0.6}Sr_{1.4}CuO_{4-\delta}$ crystallizes in the **T** structure, even though Nd_2CuO_4 forms in the **T′** phase. $Sr_3Ti_2O_7$-type structure intervenes between the **T′** and **T** structures, and unknown second phases have been also identified (4) in this intermediate range. The $Nd_2SrCu_2O_6$ phase and the $Nd_{1.2}Sr_{1.8}Cu_2O_{6-\delta}$ phase, both having the $Sr_3Ti_2O_7$-type structure, have been described for $0.6 < y < 0.8$ in $Nd_{2-y}Sr_yCuO_{4-\delta}$. For $Gd_{2-y}Sr_yCuO_4$ (5), the **T′** phase is retained along $0 \leq y \leq 0.05$, a single **T*** phase appearing for $0.35 \leq y \leq 0.45$ and the 213 phase for $0.8 \leq y \leq 1$. In this system, the **T** phase is not encountered probably due to the smaller ionic size of Gd^{3+} with respect to those of Nd^{3+} and Pr^{3+}.

A structural study in the $Pr_{2-y}Sr_yCuO_4$ system (6, 7) suggests a more complex situation, since a structural evolution **T′–T*–T–213** phase is observed with increasing Sr substitution. Single-phase materials showing these structures in the system were synthesized for $0 \leq y \leq 0.1$, $y = 0.4$, $y = 1$, and $y = 2$, respectively.

In order to understand the relationship among Sr content, oxygen content, microstructure, and stability range of **T′**, **T***, and **T** phases in the $Pr_{2-y}Sr_yCuO_{4-\delta}$ system, we have performed a selected area electron diffraction (SAED) and a high resolution electron microscopy (HREM) study of this system by preparing samples with accurate control of the oxygen content.

2. EXPERIMENTAL

Two series of $Pr_{2-y}Sr_yCuO_{4-\delta}$ ($0 \leq y \leq 2$) polycrystalline materials have been prepared by solid state reaction in alumina crucibles:

(i) Materials prepared in air were obtained by heating stoichiometric amounts of Pr_6O_{11} (previously dried at 900°C), $SrCO_3$, and CuO, in air at 900°C for 12 hr. The product was fired at 1100°C for four days with intermediate grindings.

(ii) Oxidized materials were prepared by heating the previously air-synthesized materials under O_2 atmosphere at 1100°C for three days.

The average cationic composition was determined by inductive coupling plasma (ICP). Thermogravimetric analysis was performed on a thermobalance based on a CAHN D-200 electrobalance which allows one to appreci-

[1] To whom correspondence should be addressed.

0022-4596/95 $6.00

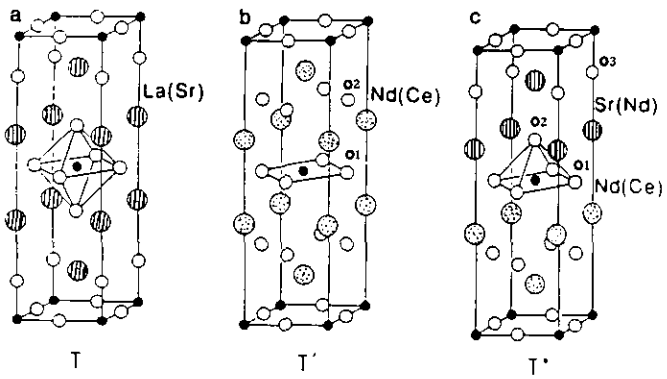

FIG. 1. The structures of (a) **T** phase, (b) **T'** phase, and (c) **T*** phase.

TABLE 2
Phases Encountered by X Ray Diffraction and Unit Cell Parameters of Air-Synthesized $Pr_{2-y}Sr_yCuO_{4-\delta}$ Materials

y	Phase	**a** (nm)	**b** (nm)	**c** (nm)	V (nm^3)
0.0	**T'**	0.3959(2)		1.226(2)	0.1920
0.10	**T'** + R_2	0.3960(1)		1.221(3)	0.1914
0.25	**T'** + **T***				
0.4	**T***	0.3861(3)		1.249(2)	0.1863
0.45	**T*** + **T**				
1.0	**T**	0.3739(2)		1.289(1)	0.1802
1.5	**T** + **(213)**				
2.0	**(213)**	0.3496(2)	0.3910(2)	1.269(2)	0.1735

Note. R_2: minority secondary phase.

ate variations of the oxygen content within $\pm 5 \times 10^{-3}$ on a sample of about 100 mg. The overall oxygen content was determined thermogravimetrically by reduction at 800°C under 0.3 H_2/0.2 He atmosphere. The Cu oxidation degree was determined by iodometric titration.

Powder X ray diffraction (XRD) patterns were performed on a SIEMENS D-5000 diffractometer using Cu$K\alpha$ radiation. SAED and HREM were performed on both JEOL 2000FX and JEOL 4000EX electron microscopes.

3. RESULTS AND DISCUSSION

A. Materials Prepared in Air

Chemical analysis by iodometric titration shows the presence of both Cu^{2+}/Cu^{3+} in Sr-doped materials. Table 1 shows both the average oxidation state of Cu and the oxygen content of samples. From these values it can be deduced that in all monophasic materials, Pr is in oxidation state III, the partial substitution of Pr^{3+} by Sr^{2+} leading to an increase of the Cu average oxidation state when the oxygen stoichiometry is close to 4. For $y \geq 1$, the Cu oxidation state decreases and a considerable amount of anionic vacancies is obtained.

TABLE 1
Average Oxidation State of Cu and Oxygen Content of Air-Synthesized $Pr_{2-y}Sr_yCuO_{4-\delta}$ Materials

y	δ	Cu^{+x}	Composition
0.0	0.00	2.0	$Pr_2CuO_{4.00}$
0.10	0.01	2.1	$Pr_{1.90}Sr_{0.10}CuO_{3.99}$
0.25[a]	0.02	2.2	$Pr_{1.75}Sr_{0.25}CuO_{3.98}$
0.40	0.06	2.3	$Pr_{1.60}Sr_{0.40}CuO_{3.94}$
0.45[a]	0.04	2.3	$Pr_{1.55}Sr_{0.45}CuO_{3.96}$
1.00	0.40	2.2	$PrSrCuO_{3.60}$
1.50[a]	0.57	2.3	$Pr_{0.50}Sr_{1.50}CuO_{3.43}$
2.0	1.00	2.0	$Sr_2CuO_{3.00}$

[a] Two phases.

The powder X ray diffraction study indicates that several phases appear as a function of **y**. Unit cell parameters are listed in Table 2. It is worth recalling that a **T'** single phase is only obtained for $0 \leq y \leq 0.1$. For higher Sr amounts ($y = 0.4$ and 1), the stabilization of phases presenting A cations with higher coordination of (**T*** and **T**, respectively) is favored. The materials in the intermediate range are consistent with mixture of two nearby phases.

In order to determine the accommodation of compositional variations, a SAED study was performed. For $y = 0.1$, the material with the composition $Pr_{1.9}Sr_{0.1}CuO_{3.99}$ presents a tetragonal symmetry. Although once again the X ray study suggests that a homogeneous material has been obtained, the corresponding SAED study shows the existence of two different kinds of crystal:

—A majority fraction of crystals shows diffraction maxima which can be indexed on the basis of a tetragonal **T'** cell, according to the X ray diffraction data.

—All SAED patterns corresponding to the second type of crystals can be assigned to the oxygen-deficient $n = 2$ term of the Ruddlesden and Popper series (8) with the composition $(PrSr)_{n+1}Cu_nO_{3n+1}$ and parameters, **a** = 0.396

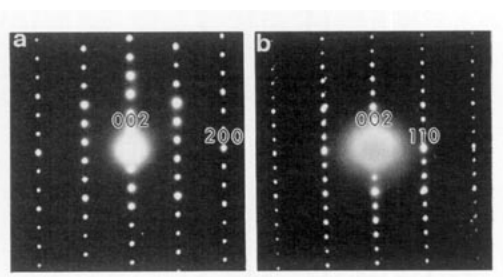

FIG. 2. SAED patterns of $Pr_{1.9}Sr_{0.1}CuO_{3.99}$ along (a) [010] and (b) [$\bar{1}$10].

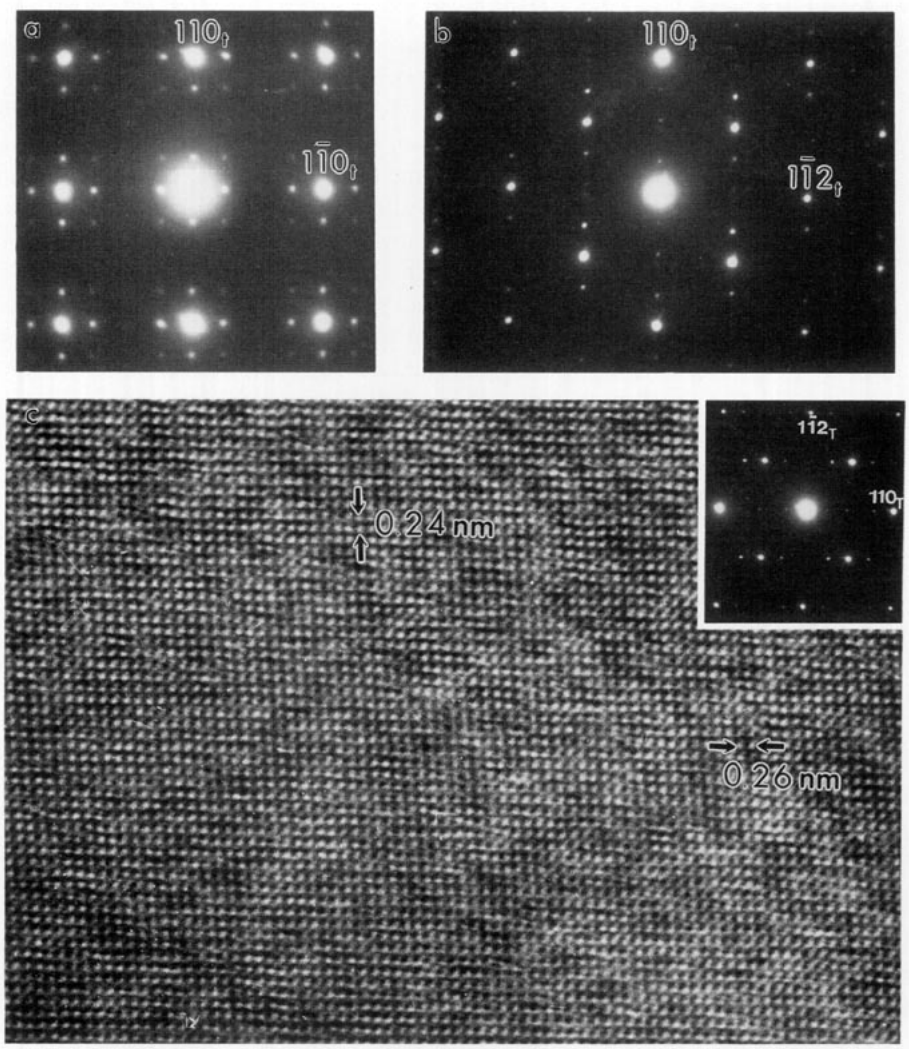

FIG. 3. SAED patterns of $PrSrCuO_{3.60}$ along (a) $[001]_t$, and (b) $[\bar{1}11]_t$; (c) HREM image corresponding to the $[\bar{1}11]_t$ zone axis.

nm and **c** = 1.954 nm, isostructural with $La_{2-x}A_{1+x}Cu_2O_{6-x/2}$ (A = Sr, Ca) (9). Figure 2 shows the SAED patterns along [010] and [$\bar{1}$10] zone axes. It is worth mentioning that the EDS analysis of this type of crystal shows a Sr and Cu excess leading to the composition of $Pr_{1.8}Sr_{1.2}Cu_2O_z$, according to which the y = 0.1 material is constituted by a majority fraction of crystals with the composition $2:1:4-\delta$ and a minority fraction of crystals with the composition $3:2:7-\delta$.

For y = 0.4, the powder X ray diffraction study indicates that another structural transition takes place, since a material showing the tetragonal $P4/nmm$ symmetry characteristic of the **T*** structural type is obtained. All SAED patterns observed can be indexed on the basis of this type. These results indicate that no additional order is found. Accordingly, it can be deduced that nonstoichiometry is probably accommodated by means of random distribution of oxygen vacancies. If some ordering exists, it would be highly nonperiodic and its contribution to the diffraction would appear only in the incoherent background between Bragg reflections.

The SAED study of $PrSrCuO_{3.6}$ shows that besides the basic spots corresponding to the **T** structure observed as single phase in the X ray diffraction study, superstructure weak reflections are seen in all crystals. Figure 3a shows the SAED pattern along the $[001]_t$ zone axis (subindex t refers to the K_2NiF_4 tetragonal cell). Weak first-order satellite reflections in all crystals observed along both [110] and [1$\bar{1}$0] directions suggest that these crystals have an incommensurable modulated structure. Moreover, very weak second-order satellites are also seen. Figure 3b shows the SAED pattern along the $[\bar{1}11]_t$ zone axis,

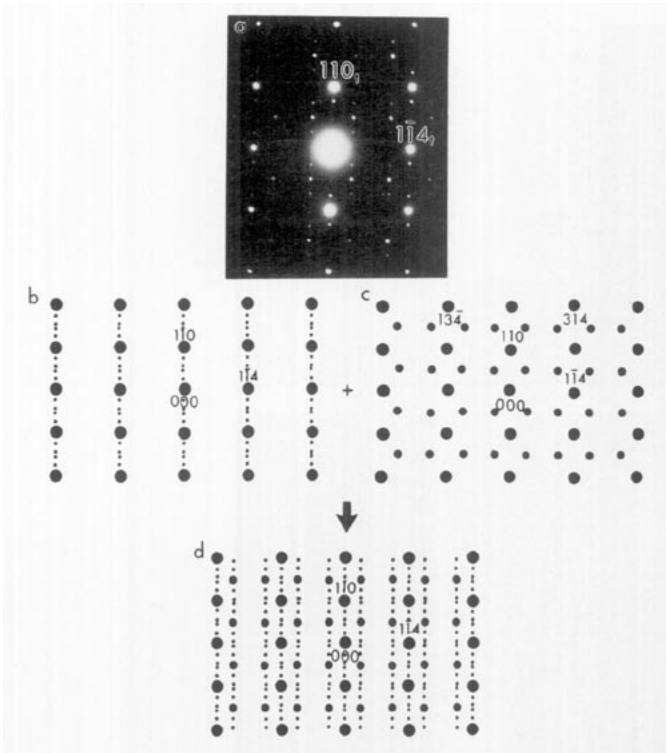

FIG. 4. (a) SAED pattern of $PrSrCuO_{3.60}$ along the $[2\bar{2}1]_t$ zone axis. (b), (c), and (d) schematic representation of the different superstructure maxima.

where the second-order satellites are more clearly seen along the $[110]_t$ direction. The modulation period for these incommensurable crystals is 4.3. The HREM micrograph with the electron beam along $[\bar{1}11]$ (Fig. 3c) clearly shows the modulation along [110].

Figure 4a shows the SAED pattern along the $[2\bar{2}1]_t$ zone axis. Three types of diffraction maxima can be recognized:

(a) Very strong reflections characteristic of the tetragonal **T**-type substructure.

(b) A series of maxima of lower intensity corresponding to the first- and second-order satellites along $[110]_t$ as schematized in Fig. 4b.

(c) Another set of satellite reflections can be observed along $[314]_t$ and $[13\bar{4}]_t$ (schematically shown in Fig. 4c). The overlapping of these series of maxima leads to the pattern schematically represented in Fig. 4d which is coincident with the experimental SAED pattern shown in Fig. 4a.

Figure 5a shows the SAED pattern along $[010]_t$. Weak first- and second-order satellite reflections can be observed along $[100]_t$. The modulation period is 2.11. Although the HREM micrograph along $[010]_t$ (Fig. 5b) does not clearly show the existence of such a modulation, when the sample is left for a few minutes within the microscope under normal observation conditions the reduction process induced under the electron beam leads to an increase of the modulation. (Fig. 5c). On the basis of this information, it seems that short distance ordering of anionic vacancies is responsible for such a modulation. Although it is complicated to propose a structural model consistent with the accommodation of anionic vacancies in $PrSrCuO_{3.6}$, the SAED study suggests that oxygen vacancies should be ordered along the basal plane corresponding to $[CuO_6]$ octahedra leading to an incommensurate modulated superstructure along $[100]_t$, $[110]_t$, and equivalent directions of **T** phase.

It is worth recalling that a previous SAED study (2, 10) of the $La_{2-y}Sr_yCuO_{4-\delta}$ system for $1 \leq y \leq 1.34$ shows superstructure spots along $[100]_t$ and $[010]_t$ directions of the **T**-type structure leading to a tetragonal cell with parameters $\mathbf{a} = na_t$ and $\mathbf{c} = c_t$, a_t, and c_t being the **T**-type unit cell parameters and n an integer or fractionary which depends on the Sr composition. According to these authors, this kind of superstructure seems to be due to the ordering of oxygen vacancies in O1 sites which are situated along the basal plane of CuO_6 octahedra. However, no relationship between oxygen content and microstructure was established.

According to X ray and neutron diffraction studies (6), any possibility of ordering in the **T**-phase $PrSrCuO_{3.6}$ is ruled out. However, some kind of ordering is detected by electron diffraction, as shown above. Moreover, neutron diffraction studies performed in the isostructural $Nd_{2-y}Sr_yNiO_{4-\delta}$ system (11) show evidence of some ordering of oxygen vacancies along [110].

B. Oxidized Materials

Air-prepared materials were oxidized under O_2 atmosphere at 1100°C. Table 3 shows the average chemical composition and phases observed by X ray diffraction as a function of δ. The diffractometric study shows the appearance of two new single phases.

For $y = 0.45$, a **T***-related material with orthorhombic symmetry arises with unit cell parameters, $\mathbf{a} = 0.5469$ nm, $\mathbf{b} = 0.5516$ nm, and $\mathbf{c} = 1.248$ nm, which will be called **T***(o) in the following.

On the other hand, the powder X ray diffraction pattern of $y = 1$ material shows a series of maxima which cannot be assigned to neither of the up to now **T**-related phases described. In order to solve the unit cell corresponding to this material a SAED study was performed.

As a first conclusion of such a study, it is worth recalling that only one kind of crystal was detected. Figure 6a shows the SAED pattern along the [001] zone axis, where besides the strong maxima corresponding to the previous

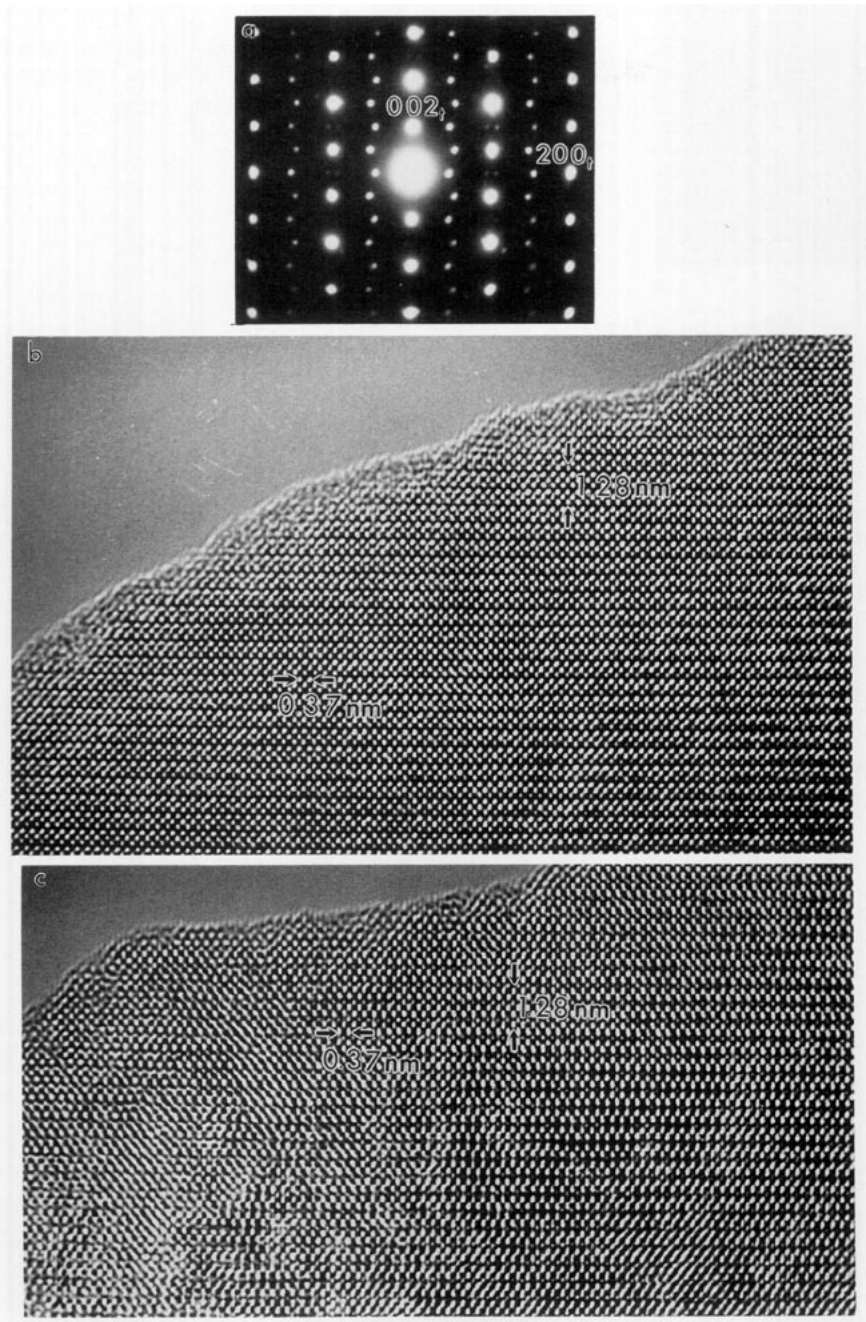

FIG. 5. (a) SAED pattern of $PrSrCuO_{3.60}$ along the $[010]_t$ zone axis. (b) Corresponding HREM image. (c) HREM along the same projection after a few minutes under the electron beam.

orthorhombic cell, a set of maxima of very weak intensity can be observed along [010]. These spots are due to the existence of a twin involving a 90° rotation, as schematically shown in Fig. 6b. Figure 7a shows the SAED pattern along the [100] zone axis. The corresponding HREM image is shown in Fig. 7b.

The EDS analysis of those crystals shows a Sr and Cu excess with respect to the A_2BO_4 stoichiometry leading to the composition of $Pr_{2-y}Sr_{1+y}Cu_2O_{6-y/2}$ ($0.6 \leq y \leq 0.85$). On the basis of this information and considering that the average composition as deduced by ICP and thermogravimetric analysis is $PrSrCuO_{3.84}$, an excess of a praseodymium oxide should appear to justify the formation of a phase with the cationic ratio $2 - y : 1 + y : 2 : 6 - y/2$. According to these results, the powder XRD pattern in Fig. 8 can be indexed on the basis of a unit cell with

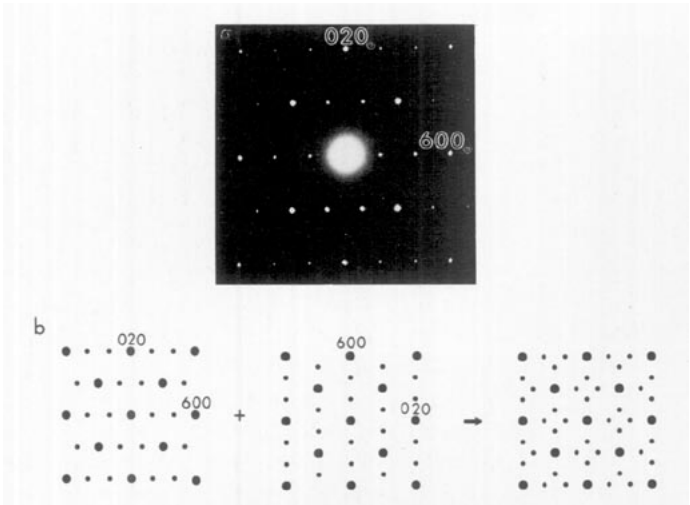

FIG. 6. (a) SAED pattern of $PrSrCuO_{3.84}$ along the $[001]_t$ zone axis and (b) schematic representation of a twin involving a 90° rotation.

parameters **a** = 1.114 nm, **b** = 0.368 nm, and **c** = 2.018 nm corresponding to $Pr_{2-y}Sr_{1+y}Cu_2O_{6-y/2}$ ($0.6 \leq y \leq 0.85$). Only a very weak maximum (marked with an arrow), which could correspond to $Pr_{12}O_{22}$, can be detected in the diffraction pattern.

TABLE 3

Chemical Composition and Phases Encountered by X Ray Diffraction for Oxidized $Pr_{2-y}Sr_yCuO_{4-\delta}$ Materials

y	Composition	Phase
0.10	$Pr_{1.90}Sr_{0.10}CuO_{4.03}$	**T'** + **T***
0.25	$Pr_{1.75}Sr_{0.25}CuO_{4.00}$	**T'** + **T***
0.40	$Pr_{1.80}Sr_{0.40}CuO_{4.02}$	**T***
0.45	$Pr_{1.55}Sr_{0.45}CuO_{3.99}$	**T***(o)
1.00	$PrSrCuO_{3.84}$	R_2[a]
1.50	$Pr_{0.50}Sr_{1.50}CuO_{3.52}$	R_{2*} + (**213**)

[a] Impurity $Pr_{12}O_{22}$.

This material is isostructural to $Ln_{2-y}Sr_{1+y}Cu_2O_{6-y/2}$ (Ln = Sm, Eu, and Gd) (12) ($0.7 \leq y \leq 0.9$) (Fig. 9a), whose crystal structure is derived from that of $La_2SrCu_2O_6$ (Fig. 9b) with additional ordered oxygen vacancies in the basal copper oxygen planes, where 1/3 of the anionic sites are vacant and are situated on the double perovskite layer and around 25% of the oxygen positions are also vacant on the CuO_2 layers (9, 13). The oxygen vacancies are ordered in the double perovskite layer leading to a threefold superstructure along the **a** direction (R_{2*}).

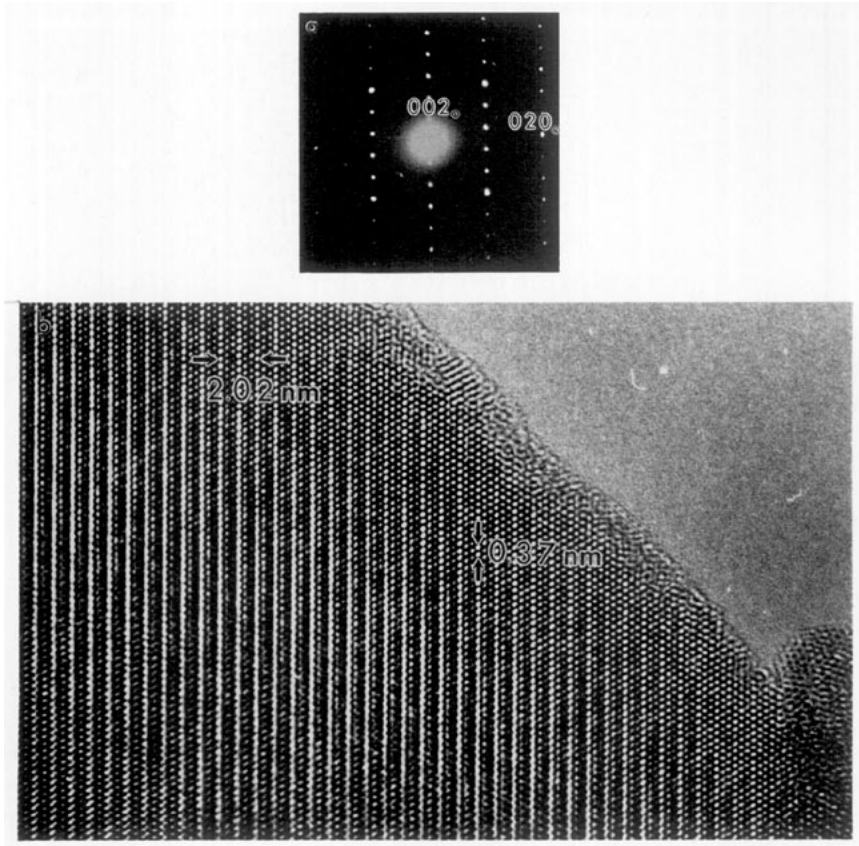

FIG. 7. (a) SAED patterns of $PrSrCuO_{3.84}$ along the $[100]_t$ zone axis and (b) corresponding HREM image.

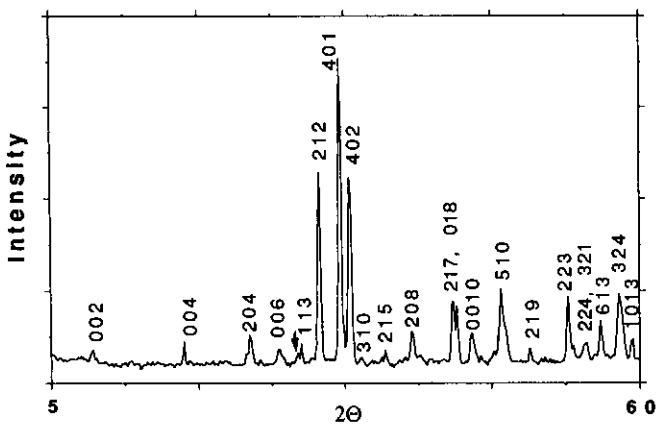

FIG. 8. X ray powder diffraction pattern of the $y = 1$ oxidized material.

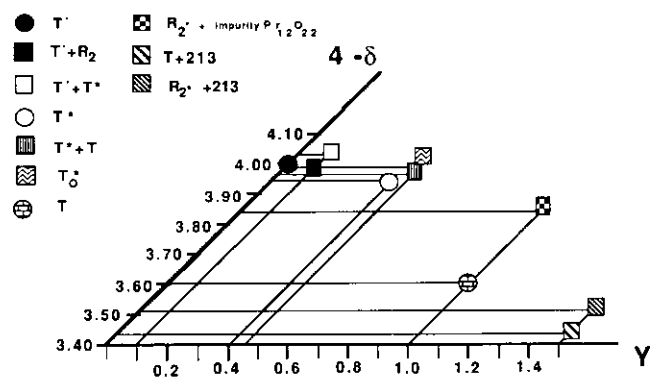

FIG. 10. Materials obtained in the $Pr_{2-y}Sr_yCuO_{4-\delta}$ system as a function of both y and δ. Circles stand for single phases.

Along the oxidation process of the $y = 1.5$ sample heated in air, the incorporation of 0.09 oxygen atoms per unit formula seems to favor, according to X ray diffraction data and in the same way that previously observed for $y = 1$, the formation of the R_2* phase, although a small amount of the **213** phase is also observed.

As a summary, Fig. 10 shows the different phases identified in the $Pr_{2-y}Sr_yCuO_{4-\delta}$ system by X ray diffraction and SAED as a function of both Sr and O content. It can be observed that an increasing of the Sr content favors the stabilization of phases **T** and **T***, i.e., those phases showing higher coordination of the *A* sites of the perovskite substructure. On the other hand, annealing under oxygen atmosphere facilitates some structural transitions.

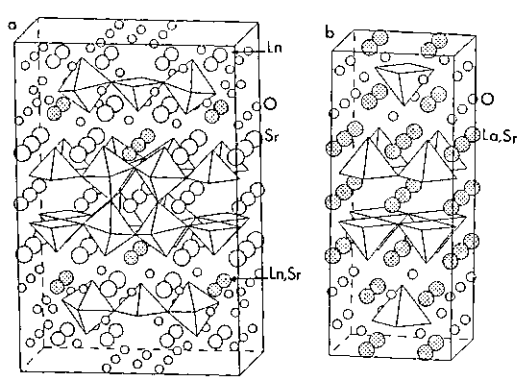

FIG. 9. Structural models of (a) $Ln_{2-x}Sr_{1+x}Cu_2O_{6-x/2}$ (Ln = Sm, Eu, and Gd) and (b) $La_2SrCu_2O_6$.

ACKNOWLEDGMENTS

Financial support from the Comisión Interministerial de Ciencia y Tecnología (CICYT, Spain) through projects MAT91-0331 and MAT93-0207 is acknowledged. We thank Dr. M. J. Sayagués and Dr. S. Nikolopoulos for helpful discussions and A. Garcia and E. Baldonedo for technical assistance.

REFERENCES

1. J. B. Goodenough, G. Demazeau, M. Pouchard, and P. Hagenmuller, *J. Solid State Chem.* **8,** 325 (1973).
2. N. Nguyen, J. Choisnet, M. Hervieu, and B. Raveau, *J. Solid State Chem.* **39,** 120 (1981).
3. K. Takahashi, B. Okai, M. Kosuge, and M. Ohta, *Jpn. J. Appl. Phys.* **27,** L1374 (1988).
4. P. H. Labbe, M. Ledesert, V. Caignaert, and B. Raveau, *J. Solid State Chem.* **91,** 362 (1991).
5. H. D. Yang, T. H. Meen, and Y. C. Chen, *Physica C* **209,** 573 (1993).
6. H. Y. Hwang, S.-W. Cheong, A. S. Cooper, Jr., L. W. Rupp, B. Batlogg, G. H. Kwei, and Z. Tan, *Physica C* **193,** 362 (1992).
7. J. Gopalakrishnan, M. A. Subramanian, C. C. Torardi, J. P. Attfield, and W. Sleight, *Mater. Res. Bull.* **24,** 321 (1989).
8. S. N. Ruddlesden and P. Popper, *Acta Crystallogr.* **11,** 54 (1958).
9. N. Nguyen, L. Er-Rakho, C. Michel, J. Choisnet, and B. Raveau, *Mater. Res. Bull.* **15,** 891 (1981).
10. N. Nguyen, F. Studer, and B. Raveau, *J. Phys. Chem. Solids* **44**(5), 389 (1983).
11. M. Medarde, J. Rodríguez-Carvajal, M. Vallet-Regí, J. M. González-Calbet, and J. Alonso, *Phys. Rev. B* **49**(13), 8531 (1994).
12. N. Nguyen, J. Choisnet, and B. Raveau, *Mater. Res. Bull.* **17,** 567 (1982).
13. D. M. De Leeuw, C. A. H. A. Mutsaers, G. P. J. Geelen, and C. Langerais, *J. Solid State Chem.* **80,** 276 (1989).